Title
Observation of an Intermediate to H_2 Binding in a Metal-Organic Framework.

Journal
Journal of the American Chemical Society, 143(36)

ISSN
0002-7863

Authors
Barnett, Brandon R
Evans, Hayden A
Su, Gregory M
et al.

Publication Date
2021-09-01

DOI
10.1021/jacs.1c07223

Peer reviewed

JACS
JOURNAL OF THE AMERICAN CHEMICAL SOCIETY
pubs.acs.org/JACS
Article

Observation of an Intermediate to H_2 Binding in a Metal–Organic Framework

Brandon R. Barnett, Hayden A. Evans, Gregory M. Su, Henry Z. H. Jiang, Romit Chakraborty, Didier Banyeretse, Tyler J. Hartman, Madison B. Martinez, Benjamin A. Trump, Jacob D. Tarver, Matthew N. Dods, Lena M. Funke, Jonas Börgel, Jeffrey A. Reimer, Walter S. Drisdell, Katherine E. Hurst, Thomas Gennett, Stephen A. FitzGerald, Craig M. Brown, Martin Head-Gordon, and Jeffrey R. Long*

Cite This: https://doi.org/10.1021/jacs.1c07223
Read Online
ACCESS | Metrics & More | Article Recommendations | Supporting Information

ABSTRACT: Coordinatively unsaturated metal sites within certain zeolites and metal–organic frameworks can strongly adsorb a wide array of substrates. While many classical examples involve electron-poor metal cations that interact with adsorbates largely through physical interactions, unsaturated electron-rich metal centers housed within porous frameworks can often chemisorb guests amenable to redox activity or covalent bond formation. Despite the promise that materials bearing such sites hold in addressing myriad challenges in gas separations and storage, very few studies have directly interrogated mechanisms of chemisorption at open metal sites within porous frameworks. Here, we show that nondissociative chemisorption of H_2 at the trigonal pyramidal Cu^+ sites in the metal–organic framework Cu^I-MFU-4*l* occurs via the intermediacy of a metastable physisorbed precursor species. *In situ* powder neutron diffraction experiments enable crystallographic characterization of this intermediate: the first time that this has been accomplished for any material. Evidence for a precursor intermediate is also afforded from temperature-programmed desorption and density functional theory calculations. The activation barrier separating the precursor species from the chemisorbed state is shown to correlate with a change in the Cu^+ coordination environment that enhances π-backbonding with H_2. Ultimately, these findings demonstrate that adsorption at framework metal sites does not always follow a concerted pathway and underscore the importance of probing kinetics in the design of next-generation adsorbents.

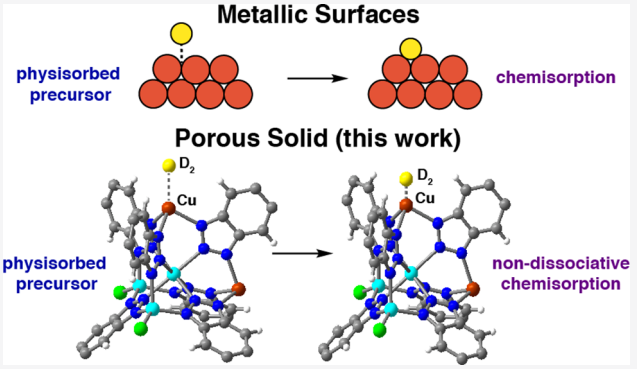

INTRODUCTION

The chemisorption of small diatomic molecules such as H_2, N_2, O_2, CO, and NO on metal surfaces has been thoroughly studied, due to its relevance to important catalytic cycles.[1,2] Many chemisorption events require that a detectable activation barrier be overcome: a process known as "activated chemisorption." Both activated and nonactivated chemisorption can involve the intermediacy of physisorbed precursor species, which represent local minima on the potential energy surface.[1−4] Evidence for precursor-mediated adsorption often relies on advanced spectroscopic or molecular beam experiments,[5,6] and the validity of adsorption pathways involving precursors has at times spurred considerable debate.[7,8]

Certain zeolites and metal–organic frameworks feature coordinatively unsaturated metal cations that can act as strong adsorption sites for various guest species, although the typically electron-poor nature of these sites tends to favor physical, rather than chemical, adsorption processes.[9−12] There has, however, been a growing interest in the synthesis of porous materials bearing electron-rich metal sites primed to engage in covalent interactions with small molecule adsorbates.[13−25] While such adsorbents may engender more exothermic adsorption and therefore higher uptake capacities, chemisorption can also give rise to transport-independent activation barriers akin to those often observed on surfaces.[1,2] An understanding of the kinetic profile for chemisorptive events within porous media is critical in the design and engineering of adsorptive storage and separation processes,[26,27] as the presence of even modest activation barriers may become

Received: July 12, 2021

https://doi.org/10.1021/jacs.1c07223
J. Am. Chem. Soc. XXXX, XXX, XXX−XXX

problematic for applications that require loading or operation at low temperatures.

To address the lack of studies examining chemisorption kinetics at open metal sites in porous solids, we have investigated the mechanism of H_2 adsorption at the trigonal pyramidal Cu^+ sites within the metal−organic framework $Cu_xZn_{5-x}Cl_{4-x}(btdd)_3$ (Cu^I-MFU-4*l*; H_2btdd = bis(1*H*-1,2,3-triazolo[4,5-*b*],[4′,5′-*i*])dibenzo[1,4]dioxin), which have previously been shown to engage in π-backbonding with H_2 and other π-acidic adsorbates.[28−32] Herein, we demonstrate that the nondissociative chemisorption of H_2 at these sites occurs through a physisorbed precursor intermediate, which is observable via powder neutron diffraction and temperature-programmed desorption. To our knowledge, this is the first crystallographic characterization of a precursor species in a chemisorption process. Computational analyses reveal that activation of H_2 is associated with a local distortion of the Cu^+ coordination environment that augments its π-backbonding capability. Together, these results holistically depict a multistep pathway for hydrogen binding that can be easily overlooked without carefully designed mechanistic investigations.

EXPERIMENTAL SECTION

General Synthesis and Characterization Methods. Unless otherwise stated, reagent-grade starting materials were purchased from commercial sources and either used as received or purified by standard procedures.[33] Solvents were sparged with Ar, dried over activated 3 Å molecular sieves, and stored in a glovebox prior to use. The framework MFU-4*l* was prepared as described previously.[34] Elemental analyses were performed in the Microanalytical Laboratory at the University of California, Berkeley. Inductively coupled plasma−optical emission spectroscopy (ICP-OES) measurements were performed on an Optima 7000 DV instrument that is maintained by the Microanalytical Laboratory. Metal−organic framework samples (1−3 mg) analyzed by ICP-OES were digested in a small amount (<1 mL) of concentrated nitric acid, and then diluted in Milli-Q ultrapure water to a concentration of 1−10 ppm Zn and Cu.

Synthesis of Cu^I-MFU-4*l*. The framework Cu^I-MFU-4*l* was synthesized using a procedure adapted from the literature.[28,30] In an N_2-filled glovebox, a *N*,*N*-dimethylacetamide (DMA) solution of $CuCl_2$ (0.275 g, 2.05 mmol, 20 eq, 20 mL) was added to activated MFU-4*l* (0.125 g, 0.100 mmol) in a 20 mL borosilicate vial. The vial was capped, placed in a hot plate well, and heated to 60 °C for 20 h. The mother liquor was subsequently decanted, and the sample was soaked in fresh DMA at 60 °C for 12 h. This process was repeated one additional time. After this second soaking, the DMA was decanted, and the framework was soaked in MeOH at 60 °C. The mother liquor was decanted and replaced with fresh MeOH three times over the course of 2 days (total of four MeOH washes). The resulting green solid was dried *in vacuo* at 60 °C in the glovebox, during which time it slowly became brown in color. The vial was then sealed and transferred to a wet, O_2-free glovebox filled with a Praxair Hydrostar (5% H_2 in N_2) gas mixture (*note*: the H_2 atmosphere is not necessary for this synthetic protocol). To the framework was added a MeOH solution of lithium formate hydrate (0.400 g, 5.71 mmol, 20 mL). The mixture was allowed to stand at room temperature for 1 h. The mother liquor was then decanted, and the framework was soaked in fresh MeOH at room temperature. This process was repeated four times over the course of 24 h (total of five MeOH washes). The framework was then dried in the glovebox *in vacuo* at 80 °C, yielding Cu^{II}-MFU-4*l*-formate as a light green powder. Autoreduction of the Cu^{2+} centers to yield Cu^I-MFU-4*l* was accomplished using a Micromeritics ASAP2020 instrument. A sample of Cu^{II}-MFU-4*l*-formate in a glass tube capped with a Transeal was heated *in vacuo* at 100 °C for 12 h, and then ramped at 2 °C/min to 180 °C, where it was held for 3 h. Between 120−180 °C, extensive offgassing occurs, and the sample changes in color from light green to beige.

Powder Neutron Diffraction Measurements. Powder neutron diffraction measurements were performed on a 0.362 g sample of Cu^I-MFU-4*l* at the National Institute of Standards and Technology Center for Neutron Research (NCNR). Data was collected at the high-resolution neutron powder diffractometer, BT1, utilizing a Ge(311) monochromator with an in-pile 60′ collimator, corresponding to a neutron wavelength of 2.0775 Å. The activated sample was loaded into a vanadium sample can in a He environment glovebox, and sealed with an indium O-ring onto a copper heating block containing a valved outlet for gas loading. After mounting the sample onto a bottom-loaded closed cycle refrigerator (CCR), the sample was cooled to base temperature for measurement. For D_2 gas dosing, the sample was connected to a fixed-volume gas manifold, heated to T = 40, 77, or 300 K, and cooled back to base temperature for measurement of Rietveld quality data collection (∼6 to ∼8 h per data set), or at the noted temperature for lattice constant determination (∼1 h per data set).

Powder neutron diffraction data were analyzed using the GSAS software suite.[35,36] Initial Le Bail refinements were first conducted to determine a background function, lattice parameters, and peak shapes.[37] The peak shape of the bare model was applied to all subsequent refinements for consistency. The position and orientation of the $btdd^{2-}$ ligands were refined using restraints to ensure planarity/bond lengths in line with chemical reasoning. The superatom approach was used to approximate the D_2 molecule as a single D atom with double occupancy.[38−40]

An extended discussion on the refinement procedures and construction of structure solutions can be found in the Supporting Information.

Solid-State Nuclear Magnetic Resonance (NMR) Spectroscopy. $^{13}C\{^1H\}$ cross-polarization magic-angle spinning (CP MAS) NMR spectra were measured on a sample of Cu^I-MFU-4*l* under an inert atmosphere. A sample of fully activated material was loaded into an airtight Teflon insert for a 4 mm rotor within the argon atmosphere of a glovebox. The closed rotor was transferred to a 11.7 T magnet and spun under continuous N_2 flow at 7.5 kHz. The magic angle (θ= 54.74°) was set prior to the experiment using KBr and the ^{13}C chemical shifts were referenced to 38.5 ppm (adamantane, tertiary carbon−higher frequency resonance).[41] A contact time of 200 μs was used, and ^1H decoupling was carried out with the TPPM pulse scheme. To determine signal intensities, the centerband and all accompanying spinning sidebands were integrated and summed up. In addition to peaks arising from the $btdd^{2-}$ carbon atoms and spinning sidebands, a small peak at 170 ppm is visible that is consistent with the formate anion.[42] Owing to the fact that no formate ligands are visible at the peripheral metal sites through powder neutron diffraction, we contend that any formate present in the material is present exclusively as "free" formate within the pores or as part of a small amount of some amorphous phase not observed in our PND refinements. Peak integration yields an upper bound value of 1 formate anion per 8 $btdd^{2-}$ ligands.

Temperature-Programmed Desorption Measurements. TPD measurements utilizing substoichiometric H_2 dosing were performed at Oberlin College. Within an argon-filled glovebox, activated Cu^I-MFU-4*l* powder (10−47 mg) was transferred to a cylindrical copper cell. In some cases, the powder was compacted inside the cell by pressing on it with a 1/8th inch diameter stainless steel rod. The compacted pellet sample could be returned to a loose powder form using a fine-tipped dental tool. All sample manipulations were performed inside the glovebox before sealing the cell using Swagelok fittings to an ORS2 bonnet valve. The sealed cell was removed from the glovebox and mounted to the base of a modified Janis ST-300T closed-cycle helium cryostat. The sample temperature was determined using a Si-diode thermometer mounted on a copper block attached to the sample cell. The temperature was maintained using a Lakeshore Model 331 controller. A small quantity (less than 0.2 mbar) of He gas was introduced to the system to ensure thermal contact between the sample and the walls of the cell. Gas dosing was performed using a Micromeritics ASAP 2020 instrument. All gases were of research grade (>99.99% purity). TPD was performed by first

https://doi.org/10.1021/jacs.1c07223
J. Am. Chem. Soc. XXXX, XXX, XXX−XXX

exposing the sample to a known amount of H_2 at a desired load temperature (20 or 293 K). The sample was then cooled at 5 K/min to a base temperature of 20 K. At this temperature, virtually all hydrogen was adsorbed. In all cases the sample was maintained at the base temperature for at least 30 min. The sample was then heated at 5 K/min while measuring the evolving gas using a Hiden Analytical "Lo MASS" series quadrupole mass spectrometer. The instrument is optimized for quantifying low mass species and has a base operating pressure of 10^{-9} Torr when used in conjunction with a low-pressure capillary orifice.

Temperature-programmed desorption (TPD) data utilizing excess H_2 were collected at the National Renewable Energy Laboratory (NREL) using a custom-built apparatus that allows for identification and quantification of effluent gases. Samples may be exposed to hydrogen (99.9999%) at pressures up to 1000 Torr, and the system can achieve pressures as low as 10^{-9} Torr. The TPD system is equipped with a mass spectrometer with detection range of 0−100 atomic mass units to detect impurities present in materials both during degas and after hydrogen exposures. In this work, the sample was initially degassed to 423 K, dosed and equilibrated over 0.4 Torr H_2 at either 76 K (the boiling point of nitrogen in Golden, CO) or room temperature. The sample was then cooled with liquid N_2, evacuated, and upon heating at 15 K/min, the H_2 desorbed was measured.

Hydrogen Adsorption Isotherm and Transient Adsorption Kinetics Measurements. UHP-grade (99.999% purity) H_2 and He were used for all adsorption measurements. Gas adsorption isotherms and transient adsorption kinetics measurements were performed using the volumetric method on a Micromeritics 3Flex gas sorption analyzer. Samples of Cu^{I}-MFU-4*l* were prepared in preweighed analysis tubes capped with a Transeal via autoreduction of Cu^{II}-MFU-4*l*-formate *in vacuo* at 180 °C (ramp rate = 2 °C/min) until the outgas rate was determined to be less than 2 μbar/min (approximately 3−4 h). The tube was then weighed and subsequently transferred to the analysis port of the instrument. Free space measurements were performed using He at the analysis temperature. A Julabo F32 water circulator was used as the isothermal bath. Oil-free vacuum pumps and oil-free pressure regulators were used for all measurements to prevent contamination of the samples, during evacuation, or of the feed gases during isotherm measurements. Adsorption kinetics measurements were performed at 276, 285, 295, and 300 K. Data at each temperature were collected in triplicate. The manifold pressure and material uptake were monitored as a function of time (0.5 Hz) using the DataMonitor software from Micromeritics. A sample of activated Cu^{I}-MFU-4*l* (0.0889 g) was loaded into a glass sample tube capped with a transeal. A glass rod of approximately equal length was inserted so as to minimize the free space within the tube. Free space measurements were performed using He at the analysis temperature. Following complete evacuation of He, the samples were dosed with 2.0 mmol/g of H_2. When adsorption over the framework sample was monitored, nearly all adsorption was seen to occur within 6 s. Accordingly, the time points between 0−6 s were utilized to construct plots of coverage versus time. The transient adsorption data were found to be modeled very well by the first-order Langmuir rate law (also known as the Lagergren expression):[43]

$$\frac{d\theta_t}{dt} = k_1(\theta_e - \theta_t)$$

in which θ_t is the fractional coverage at a given time t, θ_e is the fractional coverage at equilibrium, and k_1 is the first-order rate constant. Upon integration, this expression becomes

$$\ln(\theta_e) - \ln(\theta_e - \theta_t) = k_1 t$$

As shown in SI Figure 10, the transient adsorption data obtained for Cu^{I}-MFU-4*l* conform very well to this expression. Note that inferior fits were obtained using a second-order Langmuir kinetic expression. For an in-depth discussion on the merits of the first- and second-order kinetic expressions, see ref 43. The mean of the three rate constants determined for each run at a given temperature was used to calculate the activation barrier E_a using the Arrhenius expression

$$k_{obs} = Ae^{-E_a/RT}$$

where k_{obs} is the mean rate constant measured at each temperature T and A is the pre-exponential constant.

Density Functional Theory Calculations. Calculations were performed using a pentanuclear cluster model that represents the metal−organic framework building unit, where the $btdd^{2-}$ ligands have been truncated to benzotriazolates. The central octahedral Zn^{2+} is surrounded by four metals in trigonal coordination environments. Two of these metals are Zn^{2+} and are capped with a charge-balancing chloride. The other two metal sites are three-coordinate Cu^{+} centers. See the Supporting Information for an extended description of the methods utilized in the calculations reported herein.

Cu L-Edge X-ray Absorption Spectroscopy. Soft X-ray spectroscopy measurements at energies near the Cu L-edge were performed at bending magnet beamline 6.3.2 at the Advanced Light Source, Lawrence Berkeley National Laboratory. H_2 gas dosing experiments made use of a custom-built gas cell and similar apparatus as previously described.[44−46] Samples were deposited on X-ray transparent 150 nm thick, 2.0 mm × 2.0 mm silicon nitride windows supported by a silicon frame (Silson Ltd.). To improve adhesion of the framework to the substrate, polystyrene (M_w = 350 kg/mol, M_n = 170 kg/mol) was dissolved in toluene at a concentration of 20 mg/mL and spin coated on top of the silicon nitride windows (2000 rpm, 40 s) to form a thin polystyrene film (polystyrene exhibits minimal absorption near the Cu L-edge). Preactivated Cu^{I}-MFU-4*l* was suspended in *n*-hexane in an argon-filled glovebox, sealed in a borosilicate vial, removed from the glovebox and sonicated for 5 min. The vial was then brought back into the glovebox, and the framework was drop-cast atop the polystyrene-coated Si_3N_4 windows. After evaporation of the hexane, the window was heated *in vacuo* at 80 °C (approximately 50 mTorr) for at least 2 h. Samples were then sealed in vials and transferred to a N_2-filled glovebox where they were loaded into the gas cell and sealed before bringing to the beamline. The beamline X-ray energy was calibrated to the edge step of a Cu filter, which was set to 1.3293 nm (932.7 eV). Once attached to the beamline, the sample was pumped and kept at high vacuum (~10^{-7} Torr) for at least 30 min before any NEXAFS spectra were collected. A transmission NEXAFS spectra of the activated framework was collected before any exposure to H_2 gas. Following collection of NEXAFS spectra of the activated material, H_2 gas (Praxair, Ultra High Purity grade) was slowly introduced in the gas cell and spectra were collected *in situ* at H_2 pressures of 200, 350, 500, 750, and 1000 mbar. After gas dosing, the gas cell was pumped back down to high vacuum and a final spectrum was measured to ensure reversibility. A bare polystyrene-coated silicon nitride window was used for background correction. For normalization, a line was regressed to the pre-edge region and a polynomial regressed to the postedge region using the Athena software package.[47] The sample position was not moved during measurement to minimize effects due to spatial and thickness inhomogeneity of the drop-cast sample.

Diffuse Reflectance Infrared Spectroscopy (DRIFTS) Measurements. Infrared spectra were collected using a Bruker Vertex 70 spectrometer equipped with a glowbar source, KBr beamsplitter, and a liquid nitrogen cooled mercury−cadmium-telluride detector. A custom-built diffuse reflectance system with an IR-accessible gas dosing cell was used for all measurements. Sample temperature was controlled by an Oxford Instruments OptistatDry TLEX cryostat, and sample atmosphere was controlled by a Micromeritics ASAP 2020Plus gas sorption analyzer. In a typical experiment, activated framework material was dispersed in dry KBr (10 wt %) in an argon-filled glovebox and evacuated at room temperature overnight. Spectra were collected *in situ* under UHP-grade H_2 and D_2 (99.6 atom % D, Sigma-Aldrich) at 4 cm^{-1} resolution continually until equilibrium was observed.

https://doi.org/10.1021/jacs.1c07223
J. Am. Chem. Soc. XXXX, XXX, XXX−XXX

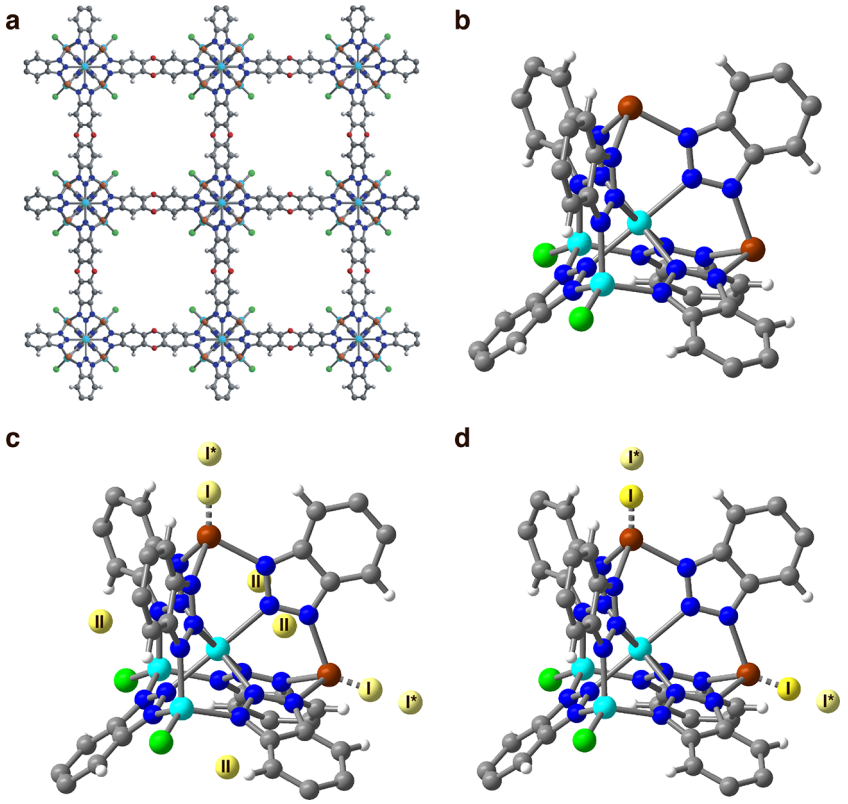

Figure 1. Crystal structures of evacuated and D_2-dosed Cu^I-MFU-4*l*. (a) A portion of the structure of activated Cu^I-MFU-4*l*, as determined from powder neutron diffraction data. (b) Expanded view of the pentanuclear nodes comprising the secondary building units of the framework. (c) Structure of Cu^I-MFU-4*l* obtained at 7 K after dosing with 0.75 D_2 molecules per Cu at 40 K and cooling to 7 K. (d) Structure obtained at 7 K following dosing with 0.75 D_2 molecules per Cu at 77 or 300 K. Cyan, brown, green, blue, gray, and white spheres represent Zn, Cu, Cl, N, C, and H atoms, respectively; yellow spheres represent isotropically refined D_2 molecules.

RESULTS AND DISCUSSION

I. *In Situ* Powder Neutron Diffraction Measurements.

The cubic metal−organic framework $Zn_5Cl_4(btdd)_3$ (MFU-4*l*) is composed of pentanuclear zinc nodes bridged by bis-triazolate $btdd^{2-}$ ligands.[34] Approximately half of its $[ZnCl]^+$ units can undergo postsynthetic cation exchange to install three-coordinate Cu^+ centers[28] that evoke the trigonal coordination geometries often observed within cuprous zeolites.[48−50] Previous work determined that this material exhibits an isosteric heat of H_2 adsorption of −32 kJ/mol, which is the most exothermic value known for molecular H_2 binding in any metal−organic framework to date.[28] We determined the crystal structure of the evacuated Cu^I-MFU-4*l* framework at 7 K using powder neutron diffraction (Figures 1a-b and S1), and the relative occupancies of the exchangeable metal sites were assigned as 55% Cu and 45% Zn based on the Cu:Zn ratio determined by inductively coupled plasma optical emission spectroscopy (ICP-OES) analysis. In all crystallographic refinements, the tetrahedral Zn^{2+} centers were found to be capped solely with a chloro ligand, which yields an overall chemical formula of $Cu_{2.2}Zn_{2.8}Cl_{1.8}(btdd)_3$.[51] This assignment is supported by $^{13}C\{^1H\}$ solid-state cross-polarization NMR and FT-IR spectroscopies, which demonstrate that any formate in the material is present in only very small relative quantities (Figures S2−3). The Fourier difference map (Figure S4) clearly shows the absence of residual density in the vicinity of the Zn−Cl moieties, demonstrating that no ligated formate is present at these sites.

Powder samples of Cu^I-MFU-4*l* were dosed with 0.75 D_2 molecules per Cu at 40 K and then cooled to 7 K for neutron diffraction data collection (Figure S5). In the resulting structure, D_2 was located ∼1.6 Å from the unsaturated Cu^+ centers (site I, Figure 1c),[52] indicating very strong binding. This value is also consistent with the Cu−H_2 distance of 1.7 Å calculated previously for the material using density functional theory (DFT),[29] but the occupancy of the site is only 0.087(18) D_2 molecules per Cu and thus represents a small fraction of the total adsorbed hydrogen (Table 1). The highest occupancy site (site II) is located at the windows of the pentanuclear tetrahedral nodes. Site II is characterized by weak physisorption and likely serves as the primary adsorption site in the parent MFU-4*l* material, for which the isosteric heat of H_2 adsorption was measured to be −5 kJ/mol at low coverage.[34]

Table 1. Occupancies of D_2 at Site I and Cubic Lattice Parameter *a*, Determined from Powder Neutron Diffraction Data Obtained after Dosing the Evacuated Framework with 0.75 eq of D_2 Per Cu at Specified Temperature[a]

Dosing Temp (K)	Site I Occupancy	*a* (Å)
40	0.087(18)	31.2174(10)
77	0.350(18)	31.1652(10)
300	0.513(14)	31.1505(6)

[a]All diffraction data were collected at 7 K, and the superatom approach was used to model D_2 molecules as isotropic D atoms.[38−40] Occupancies are expressed as molecular equivalents of D_2 per Cu. The value of *a* for the evacuated framework at 7 K is 31.2744(14) Å.

https://doi.org/10.1021/jacs.1c07223
J. Am. Chem. Soc. XXXX, XXX, XXX−XXX

One additional site (site I*) is also occupied under these conditions, located directly above site I and ~3 Å away from the strongly adsorbing Cu^+ centers.[52] Importantly, despite the difficulties posed by compositional disorder of Cu^+ and $[Zn-Cl]^+$ in this system, refinements strongly suggest that density is present at this position only following D_2 dosing. However, the compositional disorder conspires with powder averaging to obfuscate the occupancy of D_2 at site I*. Indeed, the occupancy of this site was found to be particularly sensitive to the thermal parameters employed, consistent with a significant degree of D_2 disorder or dynamics. Owing to additional compositional disorder at the metal sites, we modeled the thermal parameters of D_2 at site I* conservatively, so as to not overestimate its contribution to the total amount of adsorbed D_2 (Table S1).

The separation between sites I and I*is approximately 30% of the nearest neighbor $D_2\cdots D_2$ separation in solid D_2,[53] and thus, it is clear that both sites cannot be occupied simultaneously at a single Cu^+ center. Instead, this proximity suggests an activation barrier to D_2 binding at site I, with site I* representing a metastable physisorbed state that serves as a precursor to chemisorption. To further investigate this idea, a sample of activated Cu^I-MFU-4*l* was dosed with 0.75 D_2 molecules per Cu at successively higher temperatures (Figures S6–7). Following dosing at 77 K and subsequent cooling to 7 K, D_2 was found to occupy sites I and I* exclusively (Figure 1d and Table S1). Importantly, the occupancy of site I is much larger here than that dosed at 40 K, yet it remains significantly lower than 0.75 D_2 molecules per Cu. Increasing the dosing temperature to 300 K yields a further increase in the occupancy of site I. The increasing occupancy of site I with dosing temperature is strongly correlated with an isotropic framework contraction as shown by the decreasing value of cubic lattice parameter *a* (Table 1 and Figure S9).

Binding of H_2 at site I* can be described as a physisorbed precursor state, representing a local minimum on the potential energy surface of adsorption.[3,4,6,8] While surface science often relies on spectroscopic or molecular beam experiments to provide indirect evidence for precursor-mediated adsorption,[5,6] the spatial separation of Cu^+ centers in crystalline Cu^I-MFU-4*l* allows for the trapping and direct observation of this metastable precursor state at low temperatures. Accordingly, the kinetic nature of hydrogen adsorption at the Cu^+ sites in Cu^I-MFU-4*l* is perhaps more reminiscent of chemisorption on metallic surfaces than of the classical, barrierless physisorption generally observed within porous solids. To our knowledge, this is the first demonstration of a precursor-mediated adsorption within any porous solid.

II. Temperature-Programmed Desorption and Kinetics Measurements. Given the compositional disorder inherent to Cu^I-MFU-4*l*, we sought to experimentally probe H_2 sorption at Cu^+ in a site-specific manner. Temperature-programmed desorption (TPD) was identified as a promising technique, given the much higher temperature required for H_2 desorption from Cu^+ compared to other sites in the framework (Figure S10).[29] Accordingly, a powder sample of Cu^I-MFU-4*l* was first dosed with a known molar quantity of H_2 (substoichiometric with respect to Cu^+). For samples dosed at 293 K, the sample cell was subsequently cooled to a base temperature of 20 K prior to heating and data collection. A single high-temperature desorption feature (T_{max} = 244 K) is present following H_2 loading at 293 K (Figures 2 and S10–11). Intriguingly, however, samples that are cold-loaded with

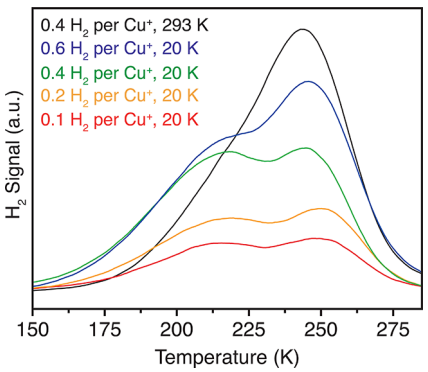

Figure 2. Temperature-programmed H_2desorption data. Thermal desorption data obtained forCu^I-MFU-4*l* after loading with H_2 at 293 or 20 K. The desorption data obtained following loading at 20 Kfeature a second, lower-temperature peak that can be assigned to desorption of H_2 directly from the physisorbed precursor state.

H_2 at 20 K give rise to a second desorption peak at a moderately lower temperature (T_{max} = 216 K) that is attributed to direct desorption from the precursor state. Importantly, this temperature is far too high to arise from desorption of H_2 that is not bound to a metal site (e.g., from crystallographic site II), as any hydrogen at such sites desorbs below 100 K (see Figure S10 and ref 29.). In agreement with the neutron diffraction results, TPD therefore indicates that low-temperature dosing inhibits binding at the thermodynamically preferred site (I) and allows for trapping of some H_2 at the precursor site (I*). However, desorption from the precursor site requires temperatures that are sufficiently high to overcome the chemisorption activation barrier, and accordingly some chemisorption does take place during the heating phase of the TPD experiment. These competing phenomena result in desorption peaks corresponding to both sites at Cu^+ being present for cold-loaded samples.

In order to estimate the activation barrier that must be overcome for hydrogen to access strong binding site I, adsorption kinetics measurements were performed between 276 and 300 K. The resulting transient adsorption data were fit to a Langmuir first-order rate law,[43] which yielded rate constants of 0.4975 s^{-1} (276 K), 0.5741 s^{-1} (285 K), 0.6435 s^{-1} (295 K), and 0.6836 s^{-1} (300 K) (Figures S13, S14). Fitting these data to the Arrhenius equation gives an activation energy (E_a) of 9 kJ/mol (Figure 3). This treatment omits the contribution that changing the temperature will have on the

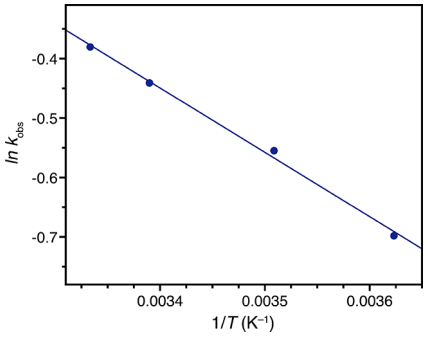

Figure 3. Arrhenius plot of the hydrogen adsorption kinetics data. Blue circles correspond to data points, while the blue line represents the least-squares linear regression. The slope of this line is equal to $-E_a/R$, where E_a is the activation energy and R is the ideal gas constant.

https://doi.org/10.1021/jacs.1c07223
J. Am. Chem. Soc. XXXX, XXX, XXX−XXX

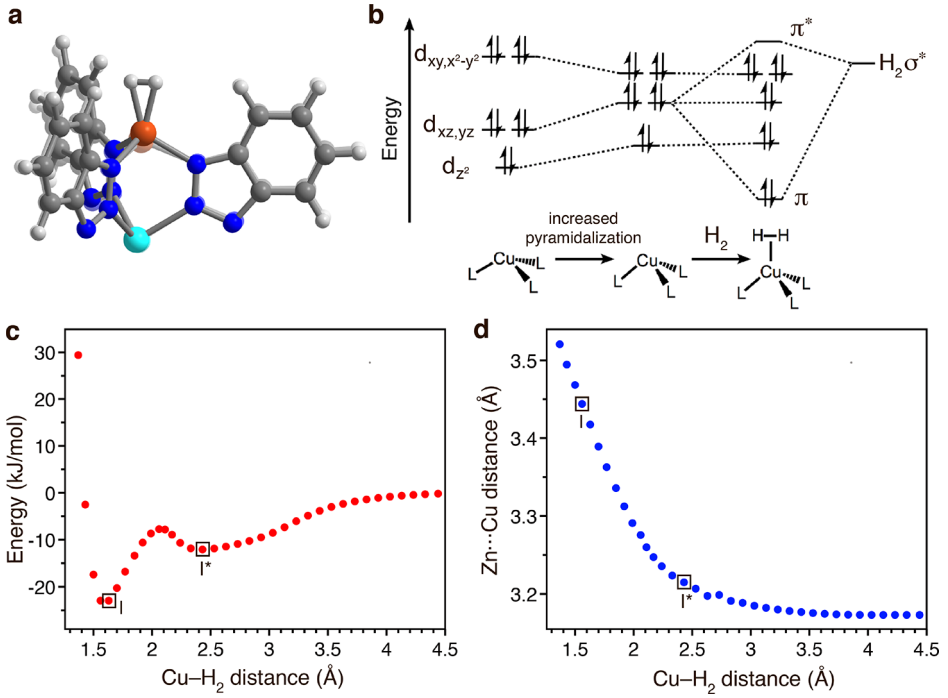

Figure 4. Structural and electronic changes associated with H_2binding in Cu^I-MFU-4*l*. (a) A portion of the DFT-optimized cluster model, with (solid structure) and without (faded structure) H_2 bound to Cu^+. (b) Qualitative molecular orbital energy diagram illustrating how the Cu 3d orbitals are affected by pyramidalization and π-backbonding to H_2. Interactions between Cu^+ and H_2 of σ symmetry are omitted for clarity. (c) Calculated potential energy surface along the Cu–H_2 coordinate at the B3LYP-D2/6-31++G**(6-31G*) level of DFT. (d) Calculated relationship between the Zn···Cu distance and Cu–H_2 distance at the B3LYP-D2/6-31++G**(6-31G*) level of DFT.

barrierless physisorption equilibrium at the precursor site,[54] and accordingly is best interpreted as a lower bound for the actual chemisorption activation barrier. Importantly, our measured lower bound value for E_a is an order of magnitude larger than the barrier to H_2 diffusion anticipated within this large-pore framework material,[55] strongly indicating that our kinetics data are reflective of a transport-independent activation barrier. The measured E_a is also too large to arise from a pathway involving H_2 desorption from site II and subsequent nonactivated chemisorption, for which the activation barrier would be equal in magnitude to the enthalpy of adsorption at site II (−5 kJ/mol).[34] Accordingly, both TPD and adsorption kinetics further substantiate the role of a precursor intermediate to hydrogen chemisorption at Cu^+, and provide support for the legitimacy of adsorption site I* in the structural model constructed from neutron diffraction data.

III. Density Functional Theory Calculations. In order to assess further the structural and electronic changes that occur upon nondissociative chemisorption at Cu^+, we performed DFT calculations on a pentanuclear cluster model that represents a single framework node (Figures S15–S17). The binding of hydrogen to Cu^+ was found to be associated with a decrease in the average framework Zn(O_h)–N distance, which can reasonably be assumed as the cause of the isotropic framework contraction given that the octahedral Zn^{2+} site represents the geometric center of the framework building unit. In addition, the calculations indicate that H_2 binding results in Cu^+ moving away from the octahedral Zn^{2+} site by ∼0.25 Å (Figures 4a and S18), resulting in an increased pyramidalization of the Cu^+ coordination sphere. This change in turn destabilizes the degenerate d_π orbitals (*e* in C_{3v} symmetry) that are of proper symmetry to form the π component of the Cu–H_2 interaction (Figure 4b). Accordingly, Cu^+ migration appears to facilitate enhanced π-backdonation to H_2. Support for this argument is found via an energy decomposition analysis[56] of the absolutely localized molecular orbitals corresponding to the Cu–H_2 bonding interaction (Table 2).

Table 2. Energy Decomposition Analyses Delineating Contributions to Binding Energy Δ*E* from Geometric Distortion, Electrostatic Interactions (Frozen), Dispersion, Polarization, Charge Transfer, and Forward and Back-Donation between Cu-Containing Node and Molecular Hydrogen at *ω* B97M-V/def2-TZVPPD (def2-SVP) Level of Theory[a]

Energy Contribution (kJ/mol)	Rigid	Relaxed
Geometric Distortion (ΔE_{gd})	1.1	17.9
Frozen (ΔE_{frz})	51.9	63.9
Dispersion (ΔE_{disp})	−23.3	−25.4
Polarization (ΔE_{pot})	−25.8	−44.5
Charge Transfer (ΔE_{ct})	−27.7	−46.1
Total (ΔE)	−23.8	−34.2
% Forward (H_2 → Cu(I))	57%	47%
% Back (Cu(I) →H_2)	43%	53%

[a]Two columns compare values for rigid versus relaxed Cu^I-MFU-4*l* node.

For a cluster with all coordinates fully relaxed, Cu → H_2 backdonation contributes −24.4 kJ/mol to the total interaction energy, which is larger than the H_2 → Cu forward donation contribution of −21.7 kJ/mol. However, for a cluster wherein only the H_2 coordinates are allowed to relax while binding to the fixed-geometry cluster (i.e., no migration of Cu^+ occurs), this analysis predicts much weaker backdonation (−11.9 kJ/mol), while forward donation decreases more modestly to

https://doi.org/10.1021/jacs.1c07223
J. Am. Chem. Soc. XXXX, XXX, XXX−XXX

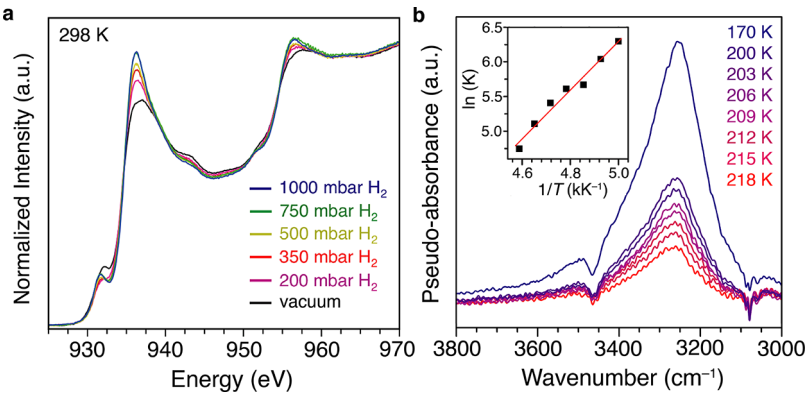

Figure 5. Spectroscopic evidence of π-backbonding. (a) *In situ* Cu L-edge X-ray absorption spectra for evacuated Cu^{I}-MFU-4*l* (black) and after dosing with various pressures of H_2 at 25 °C. (b) Fundamental ν(H−H) vibration at a constant H_2 loading at different temperatures, with the inset showing the corresponding van't Hoff plot and linear regression used to determine ΔH°_{ads} and ΔS°_{ads}.

−15.8 kJ/mol. Accordingly, these results illuminate an intricate relationship between local structural effects contributing to Cu−H_2 π-backbonding and the contraction of the larger three-dimensional framework.

A scan of the potential energy surface (PES) along the Cu−H_2 coordinate revealed a local minimum corresponding to a physisorbed precursor (Figure 4c), albeit under rather specific basis set conditions. At the B3LYP-D2/6-31++G**(6-31G*) level of theory, the optimized structure of the species corresponding to this local minimum shows H_2 bound end-on (Figure S19) with a Cu−H_2(centroid) distance of 2.43 Å (Figure 4c). Importantly, the central Zn···Cu distance in this structure is nearly unchanged from that without H_2 present. As shown in Figure 4d, Cu^{+} migration occurs at increasingly shorter Cu−H_2 distances, with the potential energy saddle point occurring at Zn···Cu distance of 2.28 Å, corresponding to a Cu−H_2 separation of 2.06 Å. The calculated barrier separating the shallow well of this local minimum structure from that of the chemisorbed species is 4.4 kJ/mol, which is smaller than the lower bound of 9.0 kJ/mol measured experimentally via adsorption kinetics (*vida supra*). Analogous scans of the PES using the def2-TZVPPD(def2-SVP) basis set yield only a shoulder, rather than a true minimum, at Cu−H_2(centroid) distances between 2 and 3 Å (Figure S20). The difficulties in quantitatively modeling the kinetic pathway of H_2 chemisorption can likely be traced to the increased flexibility available to a single cluster node relative to the extended lattice. Unfortunately, calculation of the PES using a larger computational model that mimics the extended lattice would not be tractable with the modern range separated hybrid functionals employed here. Nevertheless, it is notable that qualitative evidence for precursor-mediated chemisorption can be garnered through analysis of a single cluster node, and these data suggest that the experimental kinetic pathway arises from both local and long-range structural effects.

IV. Spectroscopic Evidence for π-Backbonding upon H_2 Binding. X-ray absorption spectroscopy (XAS) data were collected at the Cu L-edge for evacuated and H_2-dosed samples of Cu^{I}-MFU-4*l* to investigate experimentally the electronic character of the Cu^{+}−H_2 interaction. Importantly, XAS serves as an excellent probe of electronic perturbations of the valence d manifold.[57] The spectrum for activated Cu^{I}-MFU-4*l* displays L_3 and L_2 edge features at 936 and 956 eV, respectively (Figure 5a).[58] Given the absence of a pure 3d hole for electron excitation, these transitions arise due to mixing of Cu 3d character into vacant orbitals of largely σ* character.[59] Following *in situ* H_2 dosing at 25 °C, the L_3 and L_2 edge features shift to lower energies by approximately 0.5 and 0.7 eV, respectively, and grow in intensity with increasing H_2 pressure from 200 to 1000 mbar. On the basis of complementary H_2 adsorption isotherm data (Figure S21), only partial coverage of the Cu^{+} sites with H_2 is achieved under these conditions, and thus the edges consist of superimposed peaks from coordinatively unsaturated and H_2-bound Cu^{+} centers. Nevertheless, the increase in edge intensity with H_2 dosing can be directly traced to increased metal-to-ligand charge transfer via π-backdonation.[57,58,60]

For physisorbed H_2, the vibrational energy of the fundamental ν(H−H) band is generally modestly red-shifted relative to that of the free molecule (4050−4150 vs 4161 cm^{-1}).[61,62] In contrast, the *in situ* DRIFTS spectrum of Cu^{I}-MFU-4*l* dosed with H_2 exhibits a broad feature of weak intensity centered at 3252 cm^{-1}, corresponding to the fundamental ν(H−H) stretch (Figure 5b).[30] Using the spectrum for the D_2-dosed material as a baseline, we were able to isolate this band from framework-based vibrations and obtain a difference spectrum with peaks associated only with chemisorbed H_2 or D_2 (Figure S22). Unlike most molecular Kubas complexes,[63] Cu^{I}-MFU-4*l* offers a unique opportunity to study the thermodynamics of H_2 binding to a low-valent metal site directly and without consideration of a prior ligand dissociation step. To this end, variable-temperature DRIFTS data were collected for a sample of the H_2-dosed framework between 200 and 218 K (Figure 5b). Integration of the corresponding ν(H−H) peak enabled calculation of the fractional coverage by comparison to the peak area under saturation conditions (170 K).[64,65] A van't Hoff analysis afforded an enthalpy value ΔH°_{ads} = −28(2) kJ/mol and entropy value ΔS°_{ads} = −89(8) J/(mol·K)). These values are in good agreement with the thermodynamic parameters calculated from DFT (Table S2) and with the isosteric heat of adsorption measured previously from gas adsorption data.[28]

CONCLUSIONS AND OUTLOOK

The soft, electron-rich Cu^{+} sites present in Cu^{I}-MFU-4*l* serve as a counterpoint to the hard, Lewis acidic open metal sites accessible in many metal−organic frameworks and zeolites, and their aptitude for π-backbonding leads to nondissociative hydrogen binding via chemisorption. The resulting large magnitude of ΔH°_{ads} portends well for adsorptive hydrogen

https://doi.org/10.1021/jacs.1c07223
J. Am. Chem. Soc. XXXX, XXX, XXX−XXX

storage at ambient and even elevated temperatures.[26] However, this study clearly illustrates the kinetic complexities that can be associated with chemisorption in porous materials and reinforces the importance of analyzing adsorption kinetics in chemisorption-driven processes. All else being equal, an increase in the adsorption activation barrier from 1 kJ/mol (i.e., diffusion limited) to 9 kJ/mol (the lower bound measured here for Cu^{I}-MFU-4*l*) could significantly impact the time needed to load an adsorptive storage tank with H_2. For loading at 300 K, the Arrhenius equation predicts that the relative rate would decrease by a factor of 25. For cryogenic storage and loading at 77 K, the relative rates would differ by a prohibitive factor of 2.7×10^5. Given that loading time will be a critical parameter to minimize in the deployment of real-world adsorptive storage systems,[26] it becomes apparent that an optimal material will likely need to adsorb gas at (or very near) the diffusion limit. It is further noted that an inherent activation barrier to adsorption will augment the activation energy needed for desorption,[1] which could complicate recovery of the adsorbed gas.

Our investigation of Cu^{I}-MFU-4*l* suggests that the activation barrier (and, by extension, the role of a precursor intermediate) arises due to structural reorganization in the primary coordination sphere of copper. This comes as no surprise since even minor reorganizations can introduce barriers to metal−ligand binding in molecular species.[66] Analogous reorganizations following adsorbate loading in other frameworks may point toward an overlooked, non-concerted adsorption pathway that involves one (or more) intermediate species. We stress here that carefully designed investigations probing for metastable intermediates, frequently omitted in studies of adsorptive processes, are critical to garner a full mechanistic understanding of chemisorption. It is anticipated that physisorbed precursors will be realized as relevant intermediates in other chemisorption processes within porous solids and hope this work provides a roadmap for devising experiments that will enable their identification.

■ ASSOCIATED CONTENT

Supporting Information

The Supporting Information is available free of charge at https://pubs.acs.org/doi/10.1021/jacs.1c07223.

Experimental procedures, X-ray crystallographic information, additional temperature-programmed desorptions and spectroscopic data, and computational information (PDF)

Accession Codes

CCDC 1987754−1987758 contain the supplementary crystallographic data for this paper. These data can be obtained free of charge via www.ccdc.cam.ac.uk/data_request/cif, or by emailing data_request@ccdc.cam.ac.uk, or by contacting The Cambridge Crystallographic Data Centre, 12 Union Road, Cambridge CB2 1EZ, UK; fax: +44 1223 336033.

■ AUTHOR INFORMATION

Corresponding Author

Jeffrey R. Long − *Department of Chemistry, University of California, Berkeley, Berkeley, California 94720, United States; Materials Sciences Division, Lawrence Berkeley National Laboratory, Berkeley, California 94720, United States; Department of Chemical and Biomolecular Engineering, University of California, Berkeley, Berkeley, California 94720, United States;* orcid.org/0000-0002-5324-1321; Email: jrlong@berkeley.edu

Authors

Brandon R. Barnett − *Department of Chemistry, University of California, Berkeley, Berkeley, California 94720, United States; Materials Sciences Division, Lawrence Berkeley National Laboratory, Berkeley, California 94720, United States;* Present Address: Department of Chemistry, University of Rochester, Rochester, NY 14627, USA; orcid.org/0000-0002-3113-7347

Hayden A. Evans − *Center for Neutron Research, National Institute of Standards and Technology, Gaithersburg, Maryland 20899, United States;* orcid.org/0000-0002-1331-4274

Gregory M. Su − *Chemical Sciences Division, Lawrence Berkeley National Laboratory, Berkeley, California 94720, United States;* orcid.org/0000-0001-7495-8041

Henry Z. H. Jiang − *Department of Chemistry, University of California, Berkeley, Berkeley, California 94720, United States; Materials Sciences Division, Lawrence Berkeley National Laboratory, Berkeley, California 94720, United States*

Romit Chakraborty − *Department of Chemistry, University of California, Berkeley, Berkeley, California 94720, United States; Materials Sciences Division, Lawrence Berkeley National Laboratory, Berkeley, California 94720, United States*

Didier Banyeretse − *Department of Physics, Oberlin College, Oberlin, Ohio 44074, United States*

Tyler J. Hartman − *Department of Physics, Oberlin College, Oberlin, Ohio 44074, United States*

Madison B. Martinez − *Chemistry & Nanoscience Center, National Renewable Energy Laboratory, Golden, Colorado 80401, United States*

Benjamin A. Trump − *Center for Neutron Research, National Institute of Standards and Technology, Gaithersburg, Maryland 20899, United States*

Jacob D. Tarver − *Center for Neutron Research, National Institute of Standards and Technology, Gaithersburg, Maryland 20899, United States*

Matthew N. Dods − *Department of Chemical and Biomolecular Engineering, University of California, Berkeley, Berkeley, California 94720, United States*

Lena M. Funke − *Department of Chemistry, University of California, Berkeley, Berkeley, California 94720, United States; Department of Chemical and Biomolecular Engineering, University of California, Berkeley, Berkeley, California 94720, United States*

Jonas Börgel − *Department of Chemistry, University of California, Berkeley, Berkeley, California 94720, United States;* orcid.org/0000-0001-5301-8579

Jeffrey A. Reimer − *Materials Sciences Division, Lawrence Berkeley National Laboratory, Berkeley, California 94720, United States; Department of Chemical and Biomolecular Engineering, University of California, Berkeley, Berkeley, California 94720, United States;* orcid.org/0000-0002-4191-3725

Walter S. Drisdell − *Chemical Sciences Division, Lawrence Berkeley National Laboratory, Berkeley, California 94720, United States;* orcid.org/0000-0002-8693-4562

https://doi.org/10.1021/jacs.1c07223
J. Am. Chem. Soc. XXXX, XXX, XXX−XXX

Katherine E. Hurst − *Chemistry & Nanoscience Center, National Renewable Energy Laboratory, Golden, Colorado 80401, United States;* orcid.org/0000-0003-4596-9504
Thomas Gennett − *Chemistry & Nanoscience Center, National Renewable Energy Laboratory, Golden, Colorado 80401, United States; Department of Chemistry, Colorado School of Mines, Golden, Colorado 80401, United States*
Stephen A. FitzGerald − *Department of Physics, Oberlin College, Oberlin, Ohio 44074, United States;* orcid.org/0000-0001-9492-9256
Craig M. Brown − *Center for Neutron Research, National Institute of Standards and Technology, Gaithersburg, Maryland 20899, United States; Chemical and Biomolecular Engineering, University of Delaware, Newark, Delaware 19716, United States;* orcid.org/0000-0002-9637-9355
Martin Head-Gordon − *Department of Chemistry, University of California, Berkeley, Berkeley, California 94720, United States; Chemical Sciences Division, Lawrence Berkeley National Laboratory, Berkeley, California 94720, United States;* orcid.org/0000-0002-4309-6669
Complete contact information is available at: https://pubs.acs.org/10.1021/jacs.1c07223

Notes

The authors declare no competing financial interest.

■ ACKNOWLEDGMENTS

The authors gratefully acknowledge research support from the Hydrogen Materials − Advanced Research Consortium (HyMARC), established as part of the Energy Materials Network under the U.S. Department of Energy, Office of Energy Efficiency and Renewable Energy, Fuel Cell Technologies Office, under Contract Number DE-AC02-05CH11231. X-ray absorption spectroscopy measurements were performed at Beamline 6.3.2 of the Advanced Light Source, Lawrence Berkeley National Laboratory, supported by the Director, Office of Science, Office of Basic Energy Sciences, of the U.S. Department of Energy under Contract DE-AC02-05CH11231. H.A.E and B.A.T. were supported by an NRC/NIST Research Fellowship and a NIST Director's Postdoctoral Fellowship, respectively. G.M.S. and W.S.D. were supported by the Center for Gas Separations Relevant to Clean Energy Technologies, an Energy Frontier Research Center supported by the U.S. Department of Energy, Office of Science, Office of Basic Energy Sciences, under Award DE-SC0001015. S.A.F. thanks the U.S. National Science Foundation for funding (CHE-1565961). L.M.F. thanks the Alexander von Humboldt Foundation for a Feodor Lynen Postdoctoral Research Fellowship. J.B. acknowledges the Deutsche Forschungsgemeinschaft (DFG) for a Postdoctoral Research Fellowship. Certain commercial equipment, instruments, or materials are identified in this document. Such identification does not imply recommendation or endorsement by the National Institute of Standards and Technology, nor does it imply that the products identified are necessarily the best available for the purpose. We thank Dr. Katie R. Meihaus for editorial assistance, and Dr. Hiroyasu Furukawa and Dr. T. David Harris for helpful discussions.

■ REFERENCES

(1) Masel, R. I. *Principles of Adsorption and Reaction on Solid Surfaces*; Wiley: 1996.
(2) Kolasinski, K. W. *Surface Science: Foundations of Catalysis and Nanoscience*, 2nd ed.; Wiley: 2008.
(3) Bowker, M. The Role of Precursor States in Adsorption, Surface Reactions and Catalysis. *Top. Catal.* **2016**, *59*, 663.
(4) Brown, D. E.; Moffatt, D. J.; Wolkow, R. A. Isolation of an Intrinsic Precursor to Molecular Chemisorption. *Science* **1998**, *279*, 542.
(5) Rendulic, K. D.; Winkler, A. Adsorption and Desorption Dynamics as Seen Through Molecular Beam Techniques. *Surf. Sci.* **1994**, *299−300*, 261.
(6) Beutl, M.; Rendulic, K. D.; Castro, G. R. Does the Rotational State of a Molecule Influence Trapping in a Precursor? An Investigation of N_2/W(100), CO/FeSi(100) and O_2/Ni(111). *Surf. Sci.* **1997**, *385*, 97.
(7) Auerbach, D. J.; Rettner, C. T. Precursor States, Myth or Reality: A Perspective from Molecular Beam Studies. In *Kinetics of Interface Reactions*; Grunze, M., Kreuzer, H. J., Eds.; Springer Series in Surface Sciences, Vol. 8; Springer Verlag: 1987; pp 125−144. DOI: 10.1007/978-3-642-72675-0.
(8) Beutl, M.; Lesnik, J.; Rendulic, K. D.; Hirschl, R.; Eichler, A.; Kresse, G.; Hafner, J. There Is a True Precursor for Hydrogen Adsorption After All: The System H_2/Pd(111)+Subsurface V. *Chem. Phys. Lett.* **2001**, *342*, 473.
(9) Kulprathipanja, S., Ed.; *Zeolites in Industrial Separation and Catalysis*, 1st ed.; Wiley: 2010. DOI: 10.1002/9783527629565.
(10) Li, J.-R.; Kuppler, R. J.; Zhou, H.-C. Selective Gas Adsorption and Separation in Metal−Organic Frameworks. *Chem. Soc. Rev.* **2009**, *38*, 1477.
(11) Dincă, M.; Long, J. R. Hydrogen Storage in Microporous Metal−Organic Frameworks with Exposed Metal Sites. *Angew. Chem., Int. Ed.* **2008**, *47*, 6766.
(12) Yaghi, O. M.; Kalmutzki, M. J.; Diercks, C. S. *Introduction to Reticular Chemistry: Metal−Organic Frameworks and Covalent Organic Frameworks*; Wiley-VCH Verlag & Co. KGaA: 2019. DOI: 10.1002/9783527821099.
(13) Bloch, E. D.; Murray, L. J.; Queen, W. L.; Chavan, S.; Maximoff, S. N.; Bigi, J. P.; Krishna, R.; Peterson, V. K.; Grandjean, F.; Long, G. J.; Smit, B.; Bordiga, S.; Brown, C. M.; Long, J. R. Selective Binding of O_2 over N_2 in a Redox−Active Metal−Organic Framework with Open Iron(II) Coordination Sites. *J. Am. Chem. Soc.* **2011**, *133*, 14814.
(14) Anderson, J. S.; Gallagher, A. T.; Mason, J. A.; Harris, T. D. A Five-Coordinate Heme Dioxygen Adduct Isolated Within a Metal−Organic Framework. *J. Am. Chem. Soc.* **2014**, *136*, 16489.
(15) Reed, D. A.; Keitz, B. K.; Oktawiec, J.; Mason, J. A.; Runčevski, T.; Xiao, D. J.; Darago, L. E.; Crocellà, V.; Bordiga, S.; Long, J. R. A Spin Transition Mechanism for Cooperative Adsorption in Metal−Organic Frameworks. *Nature* **2017**, *274*, 2605.
(16) Zhang, J.-P.; Kitagawa, S. Supramolecular Isomerism, Framework Flexibility, Unsaturated Metal Center, and Porous Property of Ag(I)/Cu(I) 3,3′,5,5′-Tetrametyl-4,4′-Bipyrazolate. *J. Am. Chem. Soc.* **2008**, *130*, 907.
(17) Burgun, A.; Coghlan, C. J.; Huang, D. M.; Chen, W.; Horike, S.; Kitagawa, S.; Alvino, J. F.; Metha, G. F.; Sumby, C. J.; Doonan, C. J. Mapping-Out Catalytic Processes in a Metal−Organic Framework with Single-Crystal X-Ray Crystallography. *Angew. Chem., Int. Ed.* **2017**, *56*, 8412.
(18) Jaramillo, D. E.; Reed, D. A.; Jiang, H. Z. H.; Oktawiec, J.; Mara, M. W.; Forse, A. C.; Lussier, D. J.; Murphy, R. A.; Cunningham, M.; Colombo, V.; Shuh, D. K.; Reimer, J. A.; Long, J. R. Selective Nitrogen Adsorption via Backbonding in a Metal−Organic Framework with Exposed Vanadium Sites. *Nat. Mater.* **2020**, *19*, 517.
(19) Li, B.; Zhang, Y.; Krishna, R.; Yao, K.; Han, Y.; Wu, Z.; Ma, D.; Shi, Z.; Pham, T.; Space, B.; Liu, J.; Thallapally, P. K.; Liu, J.; Chrzanowski, M.; Ma, S. Introduction of π-Complexation Into Porous Aromatic Framework for Highly Selective Adsorption of Ethylene Over Ethane. *J. Am. Chem. Soc.* **2014**, *136*, 8654.

(20) Yoon, J. W.; Chang, H.; Lee, S.-J.; Hwang, Y. K.; Hong, D.-Y.; Lee, S.-K.; Lee, J. S.; Jang, S.; Yoon, T.-U.; Kwac, K.; Jung, Y.; Pillai, R. S.; Faucher, F.; Vimont, A.; Daturi, M.; Férey, G.; Serre, C.; Maurin, G.; Bae, Y.-S.; Chang, J.-S. Selective Nitrogen Capture by Porous Hybrid Materials Containing Accessible Transition Metal Ion Sites. *Nat. Mater.* **2017**, *16*, 526.
(21) Sato, H.; Kosaka, W.; Matsuda, R.; Hori, A.; Hijikata, Y.; Belosludov, R. V.; Sakaki, S.; Takata, M.; Kitagawa, S. Self-Accelerating CO Sorption in a Soft Nanoporous Crystal. *Science* **2014**, *343*, 167.
(22) Rieth, A. J.; Dincă, M. Controlled Gas Uptake in Metal−Organic Frameworks with Record Ammonia Sorption. *J. Am. Chem. Soc.* **2018**, *140*, 3461.
(23) Bohnsack, A. M.; Ibarra, I. A.; Bakhmutov, V. I.; Lynch, V. M.; Humphrey, S. M. Rational Design of Porous Coordination Polymers Based on Bis(Phosphine)MCl_2 Complexes That Exhibit High-Temperature H_2 Sorption and Chemical Reactivity. *J. Am. Chem. Soc.* **2013**, *135*, 16038.
(24) Braunecker, W. A.; Shulda, S.; Martinez, M. B.; Hurst, K. E.; Koubek, J. T.; Zaccarine, S.; Mow, R. E.; Pylypenko, S.; Sellinger, A.; Gennett, T.; Johnson, J. C. Thermal Activation of a Copper-Loaded Covalent Organic Framework for Near-Ambient Temperature Hydrogen Storage and Delivery. *ACS Materials Lett.* **2020**, *2*, 227.
(25) Braglia, L.; Borfecchia, E.; Maddalena, L.; Øien, S.; Lomachenko, K. A.; Bugaev, A. L.; Bordiga, S.; Soldatov, A. V.; Lillerud, K. P.; Lamberti, C. Exploring Structure and Reactivity of Cu Sites in Functionalized UiO-67 MOFs. *Catal. Today* **2017**, *283*, 89.
(26) Allendorf, M. D.; Hulvey, Z.; Gennett, T.; Ahmed, A.; Autrey, T.; Camp, J.; Seon Cho, E.; Furukawa, H.; Haranczyk, M.; Head-Gordon, M.; Jeong, S.; Karkamkar, A.; Liu, D.-J.; Long, J. R.; Meihaus, K. R.; Nayyar, I. H.; Nazarov, R.; Siegel, D. J.; Stavila, V.; Urban, J. J.; Veccham, S. P.; Wood, B. C. An Assessment of Strategies for the Development of Solid-State Adsorbents for Vehicular Hydrogen Storage. *Energy Environ. Sci.* **2018**, *11*, 2784.
(27) Martell, J. D.; Milner, P. J.; Siegelman, R. L.; Long, J. R. Kinetics of Cooperative CO_2 adsorption in Diamine-Appended Variants of the Metal−Organic Framework Mg_2(dobpdc). *Chem. Sci.* **2020**, *11*, 6457.
(28) Denysenko, D.; Grzywa, M.; Jelic, J.; Reuter, K.; Volkmer, D. Scorpionate-Type Coordination in MFU-4*l* Metal-Organic Frameworks: Small-Molecule Binding and Activation Upon the Thermally Activated Formation of Open Metal Sites. *Angew. Chem., Int. Ed.* **2014**, *53*, 5832.
(29) Weinrauch, I.; Schutz, G.; Hirscher, M.; Savchenko, I.; Mavrandonakis, A.; Heine, T.; Denysenko, D.; Volkmer, D.; Souliou, S. M.; Kim, H.-H.; Le, T. M.; Daemen, L. L.; Cheng, Y.; Ramirez-Cuesta, A. J.; Heine, T. Capture of Heavy Hydrogen Isotopes in a Metal-Organic Framework with Active Cu(I) Sites. *Nat. Commun.* **2017**, *8*, 14496.
(30) FitzGerald, S. A.; Mukasa, D.; Rigdon, K. H.; Zhang, N.; Barnett, B. R. Hydrogen Isotope Separation Within the Metal−Organic Framework Cu(I)-MFU-4*l*. *J. Phys. Chem. C* **2019**, *123*, 30427.
(31) Mohamed, M. H.; Yang, Y.; Li, L.; Zhang, S.; Ruffley, J. P.; Jarvi, A. G.; Saxena, S.; Veser, G.; Johnson, J. K.; Rosi, N. L. Designing Open Metal Sites in Metal-Organic Frameworks for Paraffin/Olefin Separations. *J. Am. Chem. Soc.* **2019**, *141*, 13003.
(32) Wright, A. M.; Sun, C.; Dincă, M. Thermal Cycling of a MOF-Based NO Disproportionation Catalyst. *J. Am. Chem. Soc.* **2021**, *143*, 681.
(33) Armarego, W. L. F.; Chai, C. L. L. *Purification of Laboratory Chemicals*, 5th ed. Elsevier, 2003.
(34) Denysenko, D.; Grzywa, M.; Tonigold, M.; Streppel, B.; Krkljus, I.; Hirscher, M.; Mugnaioli, E.; Kolb, U.; Hanss, J.; Volkmer, D. Elucidating Gating Effects for Hydrogen Sorption in MFU-4-Type Triazolate-Based Metal-Organic Frameworks Featuring Different Pore Sizes. *Chem. - Eur. J.* **2011**, *17*, 1837.
(35) Larson, A. C.; Von Dreele, R. B. *General Structure Analysis System (GSAS), Los Alamos National Laboratory Report LAUR*, **2000**, 86.
(36) Toby, H. B. EXPGUI, a graphical user interface for GSAS. *J. Appl. Crystallogr.* **2001**, *34*, 210.
(37) Le Bail, A. Whole powder pattern decomposition methods and applications: A retrospection. *Powder Diffr.* **2005**, *20*, 316.
(38) Pollock, R. A.; Her, J.-H.; Brown, C. M.; Liu, Y.; Dailly, A. Kinetic trapping of D_2 in MIL-53(Al) observed using neutron scattering. *J. Phys. Chem. C* **2014**, *118*, 18197.
(39) Wu, H.; Zhou, W.; Yildirim, T. Hydrogen storage in a prototypical zeolitic imidazolate framework-8. *J. Am. Chem. Soc.* **2007**, *129*, 5314.
(40) Brown, C. M.; Liu, Y.; Yildirim, T.; Peterson, V. K.; Kepert, C. J. Hydrogen adsorption in HKUST-1: a combined inelastic neutron scattering and first-principles study. *Nanotechnology* **2009**, *20*, 204025.
(41) Morcombe, C. R.; Zilm, K. W. Chemical shift referencing in MAS solid state NMR. *J. Magn. Reson.* **2003**, *162*, 479.
(42) Rossin, A.; Chierotti, M. R.; Giambastiani, G.; Gobetto, R.; Peruzzini, M. Amine-Templated Polymeric Mg Formates: Crystalline Scaffolds Exhibiting Extensive Hydrogen Bonding. *CrystEngComm* **2012**, *14*, 4454.
(43) Liu, Y.; Shen, L. From Langmuir Kinetics to First- and Second-Order Rate Equations for Adsorption. *Langmuir* **2008**, *24*, 11625.
(44) Drisdell, W. S.; Kortright, J. B. Gas cell for *in situ* soft X-ray transmission-absorption spectroscopy of materials. *Rev. Sci. Instrum.* **2014**, *85*, 074103.
(45) Drisdell, W. S.; Poloni, R.; McDonald, T. M.; Long, J. R.; Smit, B.; Neaton, J. B.; Prendergast, D.; Kortright, J. B. Probing adsorption interactions in metal−organic frameworks using X-ray spectroscopy. *J. Am. Chem. Soc.* **2013**, *135*, 18183.
(46) Drisdell, W. S.; Poloni, R.; McDonald, T. M.; Pascal, T. A.; Wan, L. F.; Pemmaraju, C. D.; Vlaisavljevich, B.; Odoh, S. O.; Neaton, J. B.; Long, J. R.; Prendergast, D.; Kortright, J. B. Probing the mechanism of CO_2 capture in diamine-appended metal−organic frameworks using measured and simulated X-ray spectroscopy. *Phys. Chem. Chem. Phys.* **2015**, *17*, 21448.
(47) Ravel, B.; Newville, M. Athena, Artemis, Hephaestus: Data analysis for X-ray absorption spectroscopy using IFEFFIT. *J. Synchrotron Radiat.* **2005**, *12*, 537.
(48) Fowkes, A. J.; Ibberson, R. M.; Rosseinsky, M. J. Structural Characterization of the Redox Behavior in Copper-Exchanged Sodium Zeolite Y by High-Resolution Powder Neutron Diffraction. *Chem. Mater.* **2002**, *14*, 590.
(49) Ipek, B.; Pollock, R. A.; Brown, C. M.; Uner, D.; Lobo, R. F. H_2 Adsorption on Cu(I)-SSZ-13. *J. Phys. Chem. C* **2018**, *122*, 540.
(50) Palomino, G. T.; Bordiga, S.; Zecchina, A.; Marra, G. L.; Lamberti, C. XRD, XAS, and IR Characterization of Copper-Exchanged Y Zeolite. *J. Phys. Chem. B* **2000**, *104*, 8641.
(51) See the Supporting Information for details on our choice of crystallographic model.
(52) While we can confidently assert that distinct, well-separated hydrogen binding sites lie along the same axis, Cu−D_2 bond distances have to be interpreted with caution. The disorder of Cu and Zn centers (which themselves occupy slightly different positions), the presence of apical Zn-bound chloride, and the migration of Cu^+ upon chemisorption (*vida infra*) obviate the determination of precise internuclear separations.
(53) Van Kranendonk, J.; Gush, H. P. The Crystal Structure of Solid Hydrogen. *Phys. Lett.* **1962**, *1*, 22.
(54) Wei, J. Nonlinear Phenomena in Zeolite Diffusion and Reaction. *Ind. Eng. Chem. Res.* **1994**, *33*, 2467.
(55) Saha, D.; Wei, Z.; Deng, S. Hydrogen Adsorption Equilibrium and Kinetics in Metal−Organic Framework (MOF-5) Synthesized with DEF Approach. *Sep. Purif. Technol.* **2009**, *64*, 280.
(56) Khaliullin, R. Z.; Cobar, E. A.; Lochan, R. C.; Bell, A. T.; Head-Gordon, M. Unravelling the Origin of Intermolecular Interactions Using Absolutely Localized Molecular Orbitals. *J. Phys. Chem. A* **2007**, *111*, 8753.

https://doi.org/10.1021/jacs.1c07223
J. Am. Chem. Soc. XXXX, XXX, XXX−XXX

(57) Hocking, R. K.; Wasinger, E. C.; de Groot, F. M. F.; Hodgson, K. O.; Hedman, B.; Solomon, E. I. Fe L-Edge XAS Studies of $K_4[Fe(CN)_6]$ and $K_3[Fe(CN)_6]$: A Direct Probe of Back-Bonding. *J. Am. Chem. Soc.* **2006**, *128*, 10442.
(58) Su, G. M.; Wang, H.; Barnett, B. R.; Long, J. R.; Prendergast, D.; Drisdell, W. S. Backbonding Contributions to Small Molecule Chemisorption in a Metal−Organic Framework with Open Copper(I) Centers. *Chem. Sci.* **2021**, *12*, 2156.
(59) Harkins, S. B.; Mankad, N. P.; Miller, A. J. M.; Szilagyi, R. K.; Peters, J. C. Probing the Electronic Structures of $[Cu_2(\mu\text{-}XR_2)]^{n+}$ Diamond Cores as a Function of the Bridging X Atom (X = N or P) and Charge (n= 0, 1, 2). *J. Am. Chem. Soc.* **2008**, *130*, 3478.
(60) George, S. J.; Lowery, M. D.; Solomon, E. I.; Cramer, S. P. Copper L-Edge Spectral Studies: A Direct Experimental Probe of the Ground-State Covalency in the Blue Copper Site in Plastocyanin. *J. Am. Chem. Soc.* **1993**, *115*, 2968.
(61) Vitillo, J. G.; Regli, L.; Chavan, S.; Ricchiardi, G.; Spoto, G.; Dietzel, P. D. C.; Bordiga, S.; Zecchina, A. Role of Exposed Metal Sites in Hydrogen Storage in MOFs. *J. Am. Chem. Soc.* **2008**, *130*, 8386.
(62) Kapelewski, M. T.; Geier, S. J.; Hudson, M. R.; Stück, D.; Mason, J. A.; Nelson, J. N.; Xiao, D. J.; Hulvey, Z.; Gilmour, E.; FitzGerald, S. A.; Head-Gordon, M.; Brown, C. M.; Long, J. R. M_2(*m*-dobdc) (M = Mg, Mn, Fe, Co, Ni) Metal−organic frameworks exhibiting increased charge density and enhanced H_2 binding at the open metal sites. *J. Am. Chem. Soc.* **2014**, *136*, 12119.
(63) Kubas, G. J. *Metal Dihydrogen and σ-Bond Complexes: Structure, Theory and Reactivity*; Kluwer: New York, 2001.
(64) Garrone, E.; Otero Areán, C. Variable Temperature Infrared Spectroscopy: A Convenient Tool for Studying the Thermodynamics of Weak Solid−Gas Interactions. *Chem. Soc. Rev.* **2005**, *34*, 846.
(65) FitzGerald, S. A.; Burkholder, B.; Friedman, M.; Hopkins, J. B.; Pierce, C. J.; Schloss, J. M.; Thompson, B.; Rowsell, J. L. C. Metal-Specific Interactions of H_2 Adsorbed Within Isostructural Metal−Organic Frameworks. *J. Am. Chem. Soc.* **2011**, *133*, 20310.
(66) Cammarota, R. C.; Xie, J.; Burgess, S. A.; Vollmer, M. V.; Vogiatzis, K. D.; Ye, J.; Linehan, J. C.; Appel, A. M.; Hoffmann, C.; Wang, X.; Young, V. G., Jr.; Lu, C. C. Thermodynamic and Kinetic Studies of H_2 and N_2 Binding to Bimetallic Nickel-Group 13 Complexes and Neutron Structure of a Ni(η^2-H_2) Adduct. *Chem. Sci.* **2019**, *10*, 7029.

https://doi.org/10.1021/jacs.1c07223
J. Am. Chem. Soc. XXXX, XXX, XXX−XXX